Experiments in Fluids 20 (1996) 153–164 © Springer-Verlag 1996

Droplet motion in an electrohydrodynamic fine spray

J. M. Grace and P. F. Dunn

Abstract The results of a combined experimental and numerical study on droplet behavior within an electrohydrodynamic fine spray are presented. The fine spray exists in the transition region between the multiple cone-jet and rim emission spray modes. Experiments were conducted specifically to characterize the motion of droplets within the spray. Light-sheet visualizations and measurements of droplet speed and velocity using laser-based, single-particle counters were obtained. Additionally, a numerical simulation of the droplet motion within the spray was made and compared to the experimental results. The electrohydrodynamic fine spray of ethanol droplets ($\sim$1 to 40 μm diameter) was generated using a typical capillary-plate configuration, with a capillary tip electric field intensity of $\sim 10^6$ V/m and a spray charge density of $\sim$70 C/m^3. Acquired images of the spray revealed a zone of rapid expansion near the capillary followed by a more gradual expansion farther from the capillary. *In situ* laser-diagnostic measurements confirmed these observations. Measured droplet speeds decreased rapidly with increasing axial distance from the capillary, but then increased beyond the spray's axial mid-plane as a result of a change in the sign of the axial internal electric field. Droplet axial velocity components behaved similarly. The radial velocity components exhibited a maximum value off of the spray's centerline in the near-capillary region. Farther away from the capillary, they increased monotonically with increasing radial position. These trends identified the significant role that the radial internal electric field plays in spray expansion. The numerical simulation of the normal spray verified the inferred change in sign of the axial internal field and underscored the dominant contribution of the external electric field in the near-capillary region and of the internal electric field farther away.

1 Introduction

The motion of similarly charged particles is a fundamental problem in fluid mechanics considered in many disciplines, e.g., in plasma physics where microscopic electrically charge particles are treated as a continuum or space charge (see Giles et al. 1979) or in the macroscopic domain of electrosprays where the droplets are considered part of a two-phase system (see Balachandran 1991). This paper presents the results of an experimental investigation of the motion of similarly charged droplets within an electrohydrodynamic (EHD) *fine* spray to determine how the droplet charge distribution within the spray contributes to the global droplet motion. A supplemental numerical model has been developed and is presented. The *fine* spray mode exists upon increasing the applied potential to a point slightly less than global gas breakdown. It is characterized by a polydisperse droplet population and a large spray plume with comparable radial and axial velocities (see Grace and Marijnissen 1994).

The use of an applied potential gives an additional control parameter (the droplet charge) that can be exploited for increased efficiency in the end application of a droplet spray, e.g., in paint spraying, non-impact printing and combustion. Additional applications such as lung deposition experiments (Nadarajah and Swift 1993) and high efficiency surface coatings (Shackleford 1985) take advantage of the polydisperse nature of such a spray, while applications such as microdroplet reactions benefit from high applied potentials similar to the fine spray mode (Harris et al. 1994). Continued benefits from droplet spray manipulation using the charge as a control parameter require an understanding and clarification of several outstanding issues which govern the dynamic motion of electrically charged droplets within an electrospray. For example: what forces predominate at various locations within the spray? how does the self-generated droplet internal electric field contribute to droplet motion relative to the externally imposed electric field?

An electrospray basically results from the atomization of a liquid by the action of electrical charges moving along the liquid surface under the influence of an applied electrical potential difference. Several electrical configurations for the electrospray exist, with the capillary-plate configuration being the most common (see Grace and Marijnissen 1994). In this configuration, liquid is forced through a capillary that is maintained at a high potential relative to the plate, and, upon exiting, is disrupted by electrical forces into droplets (see Lefebvre 1989; Bailey 1988).

The history of electrosprays goes back to at least 1600 when William Gilbert noticed the deformation of a liquid drop into a conical form in the presence of charged amber (Gilbert 1600). Since that time many significant developments in the field have

Received: 9 February 1995/Accepted: 17 August 1995

J. M. Grace, P. F. Dunn
Particle Dynamics Laboratory
Hessert Center for Aerospace Research
Department of Aerospace & Mechanical Engineering
University of Notre Dame
Notre Dame, IN 46556, USA

Correspondence to: P. F. Dunn

taken place. Lord Rayleigh (1882) derived the maximum charge potential that an isolated, conducting, spherical, liquid surface could sustain to balance the surface tension potential without disruption. Zelany (1914) began investigating the changes that an electrospray undergoes with an increased applied potential. Drozin 1955 catalogued these changes into 7 experimentally distinct spray variations. Taylor (1964) analytically described the stability conditions for a conical liquid surface under the action of electrical stresses. This cone, termed the Taylor cone, with a cone angle of 49.3°, is the basis for the Taylor cone spray mode (commonly referred to as the cone-jet mode). This mode represents the most frequently studied EHD spray mode. Many authors have investigated this mode (e.g., Vonnegut and Neubauer 1952; Hendricks 1962; Smith 1986; Hayati et al. 1987; Cloupeau and Prunet-Foch 1989; Tang and Gomez 1994; Rosell-Llompart and Fernández de la Mora 1994) and several models have been proposed to predict spray properties such as droplet diameter and specific charge (e.g., Pfeifer and Hendricks 1967, Gañán-Calvo et al. 1994, and Fernández de la Mora and Loscertales 1994). Despite the vast research effort on this mode, it has not fully been described for all conditions. For as much effort as has been spent on the cone-jet mode, as little has been spent on the fine spray mode due to the increased complexity. The state of electrospray research can be found from the literature, especially reviews on the EHD topic, e.g., Kozhenkov and Fuks (1976), Cloupeau and Prunet-Foch (1990) and Grace and Marijnissen (1994).

There have been few experimental investigations of the fine spray mode *per se*. Snarski and Dunn (1991) investigated the interaction of two adjacent fine sprays and Grace and Dunn (1992a) characterized the production region of the fine spray. Other investigators, e.g., Cloupeau and Prunet-Foch (1989), Hayati et al. (1987), and Lüttgens et al. (1992) have identified this spray mode through the course of describing the evolution of an EHD spray with applied voltage. None of these works fully addressed the basic physics behind the droplet behavior in this mode. Several works experimentally investigate droplet behavior in different spray modes; e.g., Tang and Gomez (1994) and Gañán-Calvo et al. (1994) in the cone-jet mode; Wang et al. (1993) in the ramified jet mode; Meesters et al. (1992) and Dunn et al. (1994) in hybrid modes that are specifically characterized by additional electrodes. Comparisons between spray modes or between different electrical configurations is difficult because of the large differences in production mechanisms and forces controlling droplet motion. This paper focuses on the motion of droplets within the spray *per se* and as such does not consider the production mechanism in any detail. Comparisons to similar electrical configurations will, therefore, be made only where applicable.

The present study, specifically, investigates experimentally the droplet behavior within the EHD fine spray in order to understand the underlying physical processes that control its structure. Additionally, this work evaluates numerically the space charge effects on droplet motion, which, although generally accepted as significant, are often neglected or globally approximated in spray modeling. Only a partial numerical solution to this inherent multi-body, elliptic problem is offered. The present model does not consider the effects of an air-phase velocity. Yet, it reveals that space charge has sufficient magnitude to influence droplet motion everywhere within the EHD fine spray and qualitatively predicts droplet velocities while quantitatively predicting droplet trajectories. The present analysis of the fine spray space charge effects also is applicable to other EHD spray modes as well as other aerosol problems of this nature. In the following, the experimental data are presented first and then discussed. Their analysis raises questions which the numerical model (presented following the experimental section) attempts to resolve. Since the model attempts to answer several questions raised by the experimental analysis, it is referred to in context rather than as an *a posteriori* discussion in the numerical section.

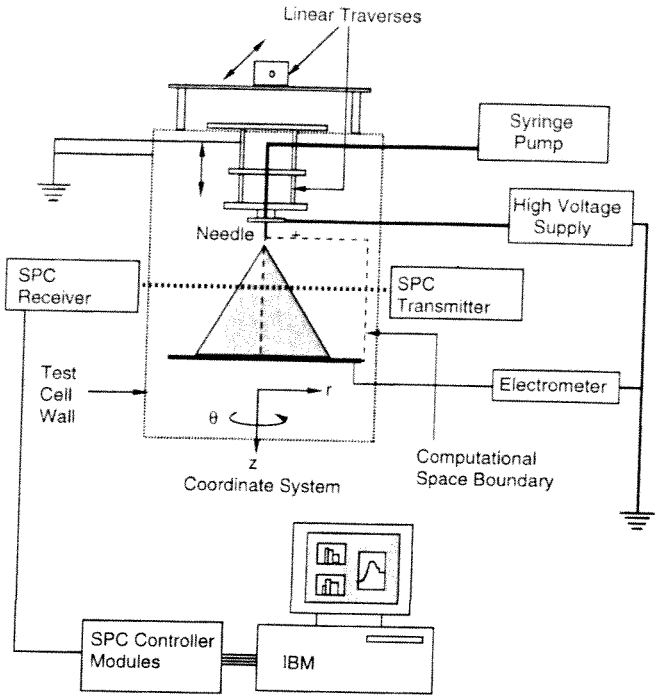

Fig. 1. Experimental apparatus

2 Experimental apparatus

The EHD fine spray was produced using a typical capillary-plate configuration, see Fig. 1. A blunt-tip, stainless-steel hypodermic needle (27 gauge: 0.0406 cm O.D., 0.0216 cm I.D. and overall length of 1.9 cm) served as the capillary, while an electrically grounded brass plate (60 cm × 60 cm) located 20 cm below the capillary tip acted as the plate. A DC high voltage supply connected in series with the capillary generated electric field intensities at the capillary tip on the order of 10^6 V/m.[1] All cases presented in this paper were conducted using an applied voltage of 15 kV (see Grace, 1993 for other cases). The working fluid, ethanol, was pumped through the capillary at a constant volumetric flow rate of $4.34 * 10^{-3}$ cc/s (ethanol properties: density, $\rho = 789$ kg/m^3, electrical conductivity, $\sigma_e = 2.0 * 10^{-5}$ S/m, surface tension $\sigma = 0.022$ N/m).

[1] The electric field is calculated using the capillary-plate approximation (Jones and Thong 1971) and constrained by the breakdown strength of air.

The spray charge density, defined as the ratio of the droplet current at the plate to the volumetric flow rate, was 70 C/m^3. The test cell dimensions were about 1.5 m on each side.

The primary measurement tool for this experiment was a laser-based, *in situ*, single-particle counter (SPC). Two individual SPC's based on different operation principles were used during the course of this investigation. The two systems were a particle-counter-sizer velocimeter (PCSV) by Insitec (1989) and a one-component phase-Doppler-particle analyzer (PDPA) by Aerometrics (1987). The classic references on these two measurement systems are those by Holve and Annen (1984) and Bachalo and Houser (1984). Each system had unique measurement capabilities (and limitations) that, when used in concert, allowed for a more thorough investigation of the EHD spray. See O'Hern and Rader (1993) for a differentiation of these and other light scattering measurement techniques. Note that the specific PCSV used for this experiment was only configured to measure droplet speed.

In addition to the SPC measurements, the global nature of the EHD fine spray was recorded using flow visualization. This flow visualization was performed using a two-dimensional sheet of laser light (see Grace and Dunn, 1992b for a description of the technique). This sheet illuminated a two-dimensional slice of the entire spray (~ 1 mm thick) at variable locations. The laser light-sheet was produced by directing the beam of a 5 W Ar-ion laser through a plano-convex cylindrical lens. The light scattered from the droplets crossing the laser light-sheet was recorded with a video camera and recorder at 30 frames/s. The video images were digitized into a personal computer using a frame grabber board and then analyzed using imaging software.

3
Experimental results

The results of this experiment are summarized in Figs. 2–8. The order in which the experimental results will be presented is as follows: first, a global flow visualization image of the spray, then the droplet speed and velocity, which represents the bulk of this study, the droplet diameter, the droplet size–velocity correlation, and finally the spray number concentration. The droplet diameter is discussed to characterize the spray mode and presented as a function of position within the spray. The size–velocity correlations and spray number concentrations are discussed in terms of the general spray nature, while the size–velocity correlation is also investigated to assess the influence of the electric field components.

3.1
Flow visualization

Figure 2 presents a digitized video image of a two-dimensional slice of the spray along the capillary axis. This image is presented to show the global scale and general expansion character of the fine spray. In addition, the spatial uniformity of the droplet streaklines and the rapid spray expansion near the needle followed by the gradual spray expansion farther from the needle is shown. These trends suggest a significant internal (or droplet) electric field effect in the region of rapid spray expansion.[2] The influence of the internal electric field on spray expansion can also be seen in Fig. 5. of Grace and Dunn (1994) where a droplet trajectory calculated using only the external field significantly under predicts the radial expansion. The spray expansion of the cone-jet mode (e.g., True 1980; Gañán-Calvo et al. 1994; Tang and Gomez 1994) does not match that of the fine spray mode due to the droplet production process in that mode where initial radial velocities as well as radial positions (relative to the scale of the production zone) can be large.

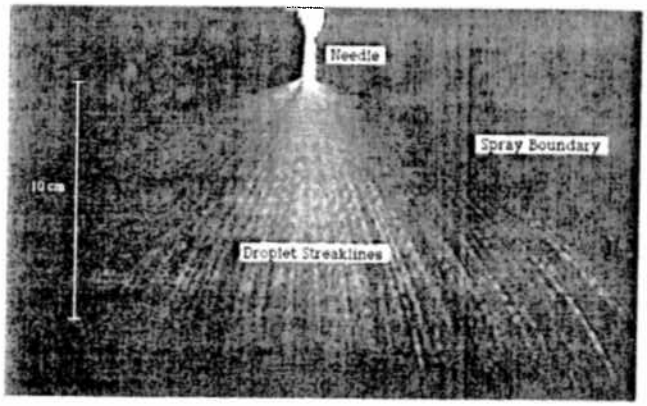

Fig. 2. Light sheet visualization of droplets in the plane of the needle's axis

3.2
Droplet speed and velocity

Figure 3 presents the average droplet speed measured using the PCSV.[3] Data were acquired at each measurement location for a specific period of time (~ 180 s). Valid data result from any droplet passing through the measurement volume in the test time and generating a scattered light signal that falls within the range of the size and speed discriminators. The discriminator ranges selected for this experiment were 2 to 50 μm for the droplet diameter and 0 to 20 m/s for the droplet speed. Note that the speeds and velocities are not normalized in this and subsequent figures because there is no accepted characteristic velocity in the fine spray mode.

The data in Fig. 3 extends axially to 15 cm from the capillary tip (3/4 of the capillary-plate spacing) and radially to regions where the measurement count rate was less than approximately 10 Hz. The spray does extend beyond the radially measured range for axial positions far from the needle tip, i.e., greater than 7 cm (see Fig. 9 which shows the reticulated, digitized spray boundary).

[2] The electric field nomenclature used in this paper defines an internal and external field, where the internal field results solely from the presence of charged droplets, and the external field results from the capillary-plate configuration and is independent of the presence of the droplets. The total electric field then is the vector sum of the internal and external fields.

[3] Speed measurements covered a larger spray domain than the velocity measurements.

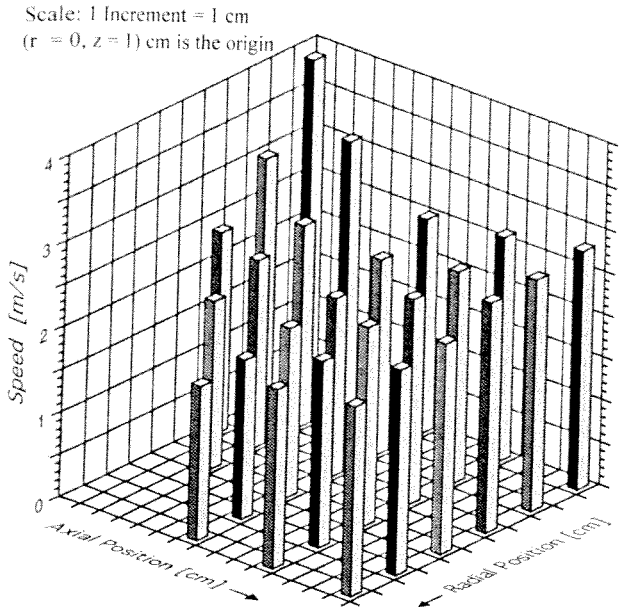

Fig. 3. Experimental droplet speed field

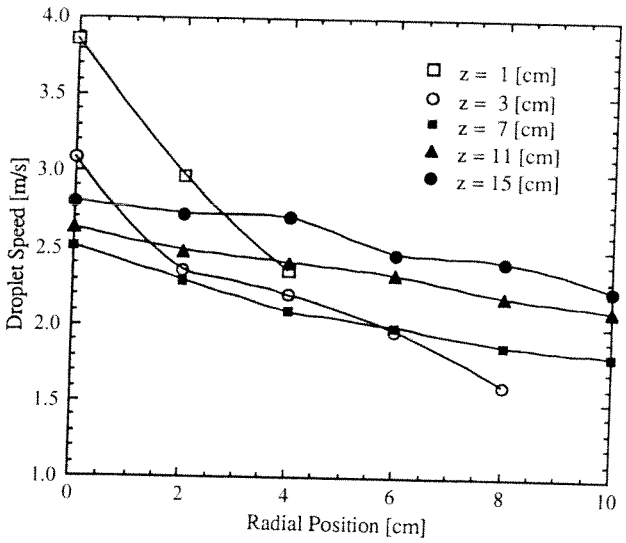

Fig. 4. Comparison of near-field and far-field experimental droplet speeds

The speed measurements presented in this figure exhibit a rapid decrease in droplet speed with distance for measurement positions near the needle, a decrease in the droplet speed with increased radial position for all axial locations, and an increase in speed with axial position, beyond the 7 cm axial station, for all radial locations. This measured speed increase with axial position is greater than the measurement uncertainty. The speed measurement technique has an uncertainty that varies with position in the spray, being greater in regions near the needle. The total uncertainty is reported as less than 8% in the near-needle region and less than 5% elsewhere in the spray (Grace and Dunn, 1992a).

Figure 4 presents the data of Fig. 3 in a two-dimensional format highlighting the variation in speed with radial position. This figure demonstrates the rapid speed decrease in the near needle region followed by the gradual decrease in the far needle region. The rapid decrease in speed with axial and radial position near the needle follows expected trends of an expanding electrospray. Here the expansion decreases both the spray kinetic energy through aerodynamic drag and the electrical potential energy through the monotonic decrease in the external field with distance from the source. The gradual decrease in speed with increasing radial position from the spray centerline far from the needle follows the slowed spray expansion and the more gradual decrease in the external electric field in this range. The increase in speed for axial positions far from the needle cannot be explained by this approach.

The results of the numerical model (see Sect. 4) suggest a mechanism responsible for the measured speed increase. The model predicted an axial velocity increase beyond the spray axial mid-plane. This was a result of a sign change in the axial internal electric field. The magnitude of the *total* axial electric field actually increased near the plate due to this internal electric field sign change. The sign change can be shown simply by considering two limiting cases. In the limit of a point very near the needle tip, all the droplets exist below this point and the internal electric field must, therefore, be directed towards the needle. In the limit of a point very near the plate, all the droplets exist above this point and the internal electric field must then be directed towards the plate.

An increase in axial velocity with approach to the plate electrode has also been reported by Gañán-Calvo et al. (1994) for the cone-jet mode. Tang and Gomez (1994) also measure droplet velocity in the cone-jet mode, but report a monotonic decrease in the axial velocity with plate approach. Although these authors also note a change in sign in the internal axial electric field (as predicted from a comparison between the experimental data and a semi-analytic external electric field), it occurs too close to the production zone to influence the droplet motion. The experimental parameters for the cone-jet modes reported in these references are slightly different than this work (lower applied voltage, lower flow rate, shorter needle-to-plate distance, larger droplet diameter, greater magnitude of the velocity, and different liquid properties), but the common ground of charged droplet motion exists.

The radial and axial component droplet velocities acquired using the PDPA are detailed in Figs 5a and 5b. These measurements cover the near needle spray region axially up to 7 cm from the needle tip and radially to 3 cm from the spray centerline for all axial positions and farther to 7 cm radial for the 7 cm axial position. These figures show that the rapid decrease in droplet speed with distance results primarily from a decrease in the axial component of the droplet velocity. The axial component exhibits the rapid decrease in magnitude in the near-needle region followed by the gradual decrease farther from the needle. The radial component exhibits a similar decrease in the rate of change with axial position; however, in this direction the velocity component is zero along the spray centerline (by symmetry) and increases with radial position. The form of the lateral velocity radial profile at the 5 mm axial station indicates that the lateral velocity reaches a maximum at some radial position and then decreases beyond this point. Similarly, the form of the lateral external electric field exhibits

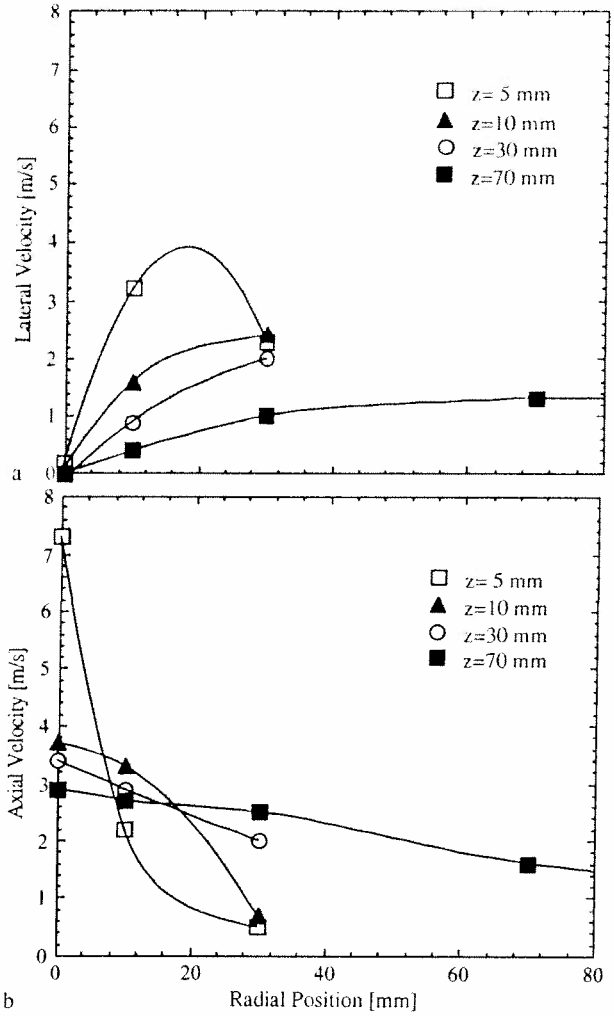

Fig. 5. **a** Experimental radial velocity versus radial position; **b** experimental axial velocity versus radial position

a local maximum off of the centerline. This electric field exhibits an off-centerline, local maximum for all axial positions, though the corresponding trend is not explicitly seen in the remaining lateral velocity data.

The numerical model showed that, in fact, this trend will not be seen in the remaining lateral velocity data. The internal lateral electric field dominated the droplet motion after a small radial distance ($r \sim 2$ cm), and this field continuously increased (beyond a small initial radius) for the spray domain. This increase in lateral internal electric field with radial position follows analogously to the sign change in the axial direction as the droplet number concentration decreases with radial position beyond a small initial radius.

Tang and Gomez (1994) also report a near-field, off-axis peak in the radial velocity profile. This peak does not disappear, rather it continues into the far field, moving to greater radial positions for increased axial positions. This work also reported that the internal radial electric field has a continuous increase with radial position. The decrease in the radial velocity profile while the internal electric field increases is not explained.

In summary, the speed and velocity results show that the EHD fine spray exhibits a source-like dispersion of droplets, rapid velocity changes in the near needle region followed by gradual changes farther from the needle, and that significant internal electric field effects are present within the spray.

3.3 Droplet diameters

Droplet diameters were measured at the same locations as the droplet component velocities using only the PDPA system. The subject spray is inherently polydisperse with diameters ranging from about 1 to about 30 μm as shown in Fig. 6. The

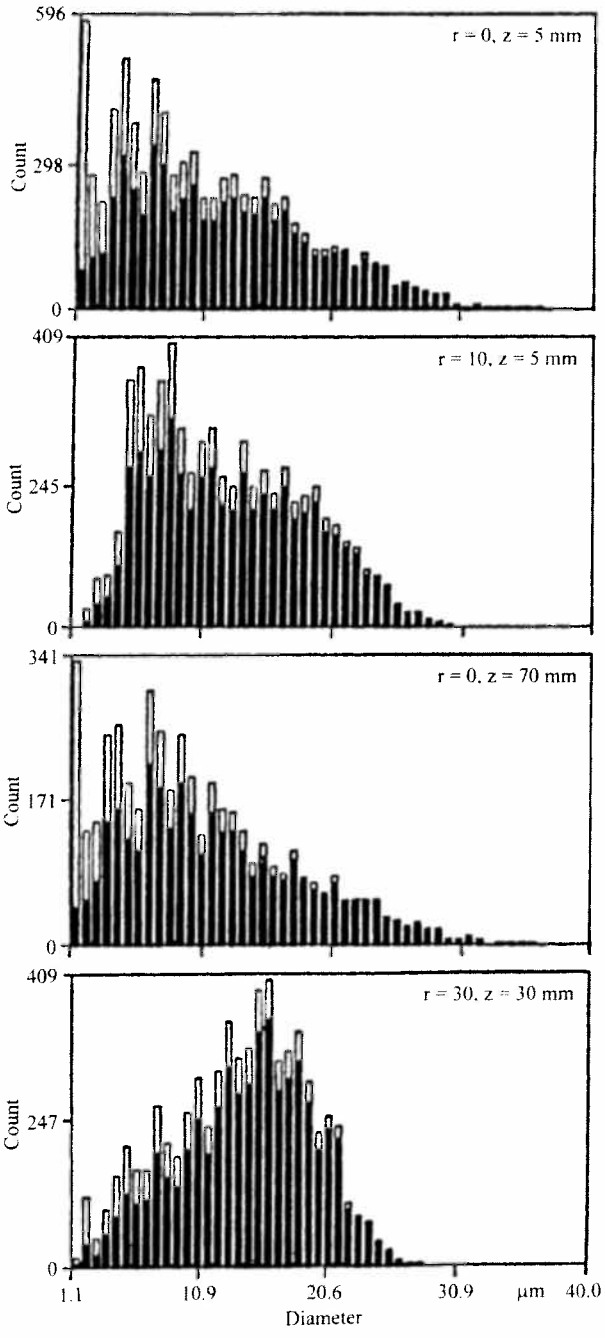

Fig. 6. Four droplet diameter distributions within the spray

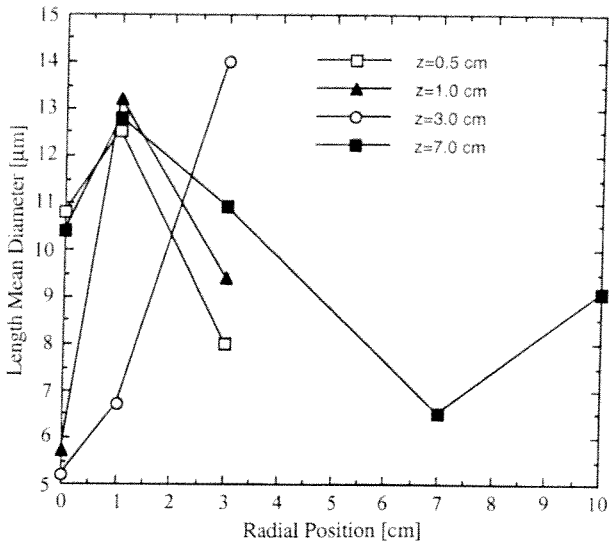

Fig. 7. Number mean droplet diameter versus radial position

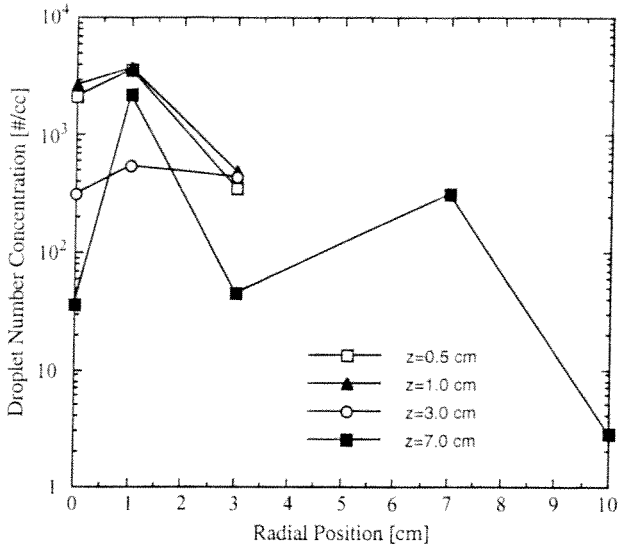

Fig. 8. Droplet number concentration versus radial position

distributions show the actual data (dark columns) and the corrected data (light columns) using an algorithm to adjust for the diameter dependence on the measurement volume (Aerometrics 1987). Here the four diameter distributions show the persistence of the polydisperse nature through the spray.

Figure 7 details the variation in the arithmetic mean droplet diameter, D_{10}, for the 14 measurement stations investigated. The curve-fits in this figure are intended only to clarify the data, not to define trends between adjacent data. From this figure a masked trend where the peak of the radial profile moves radially outward with increasing axial position can be seen, especially for the stations less than 7 cm from the needle. The $z=7.0$ cm stations and the $z=0.5$, $r=0$ cm station obscure conclusive trends, possibly due to electric field induced droplet segregation and increases to the measured diameters as a result of the production region, respectively. The radial resolution is not sufficient to discriminate between $z=0.5$ and $z=1.0$ cm at the $r=1.0$ cm position. It is sufficient to show radial motion of the peak from these two station to the $z=3.0$, $r=3.0$ cm station. This characteristic is seen for any distribution diameter, e.g., the Sauter mean diameter (D_{32}). Other cases not presented in this paper show that the trend becomes more apparent with an increase in the applied voltage (Grace 1993). This is consistent with a spray expansion where little intraspray mixing occurs, i.e., moving droplets across the streaklines in Fig. 2.

It is difficult to draw particular conclusions about droplet motion through the spray from this data, even though the data is repeatable. It does not appear that droplet evaporation plays a large role in the droplet diameter results. Indeed, tests acquired at a single spray location for over 300 s from a dry start (i.e., test cell evacuated of ethanol vapor) show identical distributions for a given time increment anywhere within the test period. The minimum time increment investigated was 20 s, which is many times shorter than the time between spray start-up and data acquisition.

3.4
Droplet number concentrations

The spray number concentration can be derived from three sources. The PDPA system measures it directly, the PCSV measures it indirectly (in this experiment), and it can be estimated from the size and velocity data coupled with the spray geometry in an order-of-magnitude sense. The last two sources would seem to be unnecessary given the direct measurement with the PDPA system. However, the number concentration results using the single component PDPA for non-principle axis measurement stations[4] were not repeatable from test to test, nor from station to station. As a result, additional methods were used to supplement the PDPA results. The velocity and diameter data were very repeatable throughout the measurements.

Figure 8 shows the number concentration results of the PDPA system as a function of radial position for the four axial measurement stations. The curves in this figure again are intended only to clarify the measurements positions rather than to define continuous trends between the discrete data. This is particularly obvious for the 7 cm axial stations where the continuous trend indicated by the curve make little sense. The results show that the number concentration generally decreases with increasing radial position while decreasing with axial distance from the needle as expected in an expanding spray. The magnitude of this data indicates a number concentration that falls within the range indicated by the two other sources considered, but does not match the high and low values. The existence of an off-centerline peak in number concentration that moves radially outward with increasing axial position, akin to the masked trend in Fig. 7, has some support, though it cannot be demonstrated effectively with the present data.

The variation in spray number concentration can also be approximated using the PCSV count rate and speed data

[4] Non-principle axis measurement stations refers to tests where the PDPA orientation did not match the major spray direction, e.g., radial measurements near the spray centerline.

through the simple algorithm C.R. $= U\ \Delta S\ n$. Here C.R. refers to the count rate, U the spray average droplet speed, n the spray average droplet number concentration and ΔS the cross-sectional area of the measurement volume. Though ΔS is implicitly a function of the droplet diameter and of the discriminator setting, it can be estimated for the dynamic range of the system[5] (Insitec 1989). The speed data smoothly progresses from near needle positions to the far field. Count rate data also follows the smooth and predictable character of the speed data, though it is not reported in this paper. Hence, the variation in droplet number concentration is taken as regular and predictable. The magnitude of the number concentrations determined in this manner are slightly lower than but on the same order as the other sources, being about 10^4 #/cc in the near field and less than 10^2 #/cc in the very far field.

The number concentration also can be estimated using an order of magnitude approach based on the spray geometry as observed through flow visualization, the known mass flow rate, and the average droplet velocity and diameter measured near the needle. Approximating the spray as a cone near the needle and considering the experimental data yields a droplet number concentration on the order of 10^4–10^5 #/cc in the near field. The averaging property of this method reduces its applicability to the far field.

Data presented by Snarski (1988) show centerline concentrations in the near field of approximately 10^4 #/cc which decrease to approximately 10^2 #/cc at the spray periphery, also in the near field. Far field data does not exist in this reference. Note that the ground electrode had a different geometry than in this work, though all other experimental conditions were identical.

In summary, all these sources support that the droplet number concentration in the fine spray mode is $\sim 10^4$–10^5 #/cc in the near field down to $\sim 10^2$ #/cc in the far field.

3.5
Droplet size–velocity correlations

The following section considers the size–velocity correlation drawn from the PDPA data. In this section, the correlation data are presented along with the limitations necessary for data interpretation. In addition, a physical interpretation of the correlations based on the governing equations is developed.

The size-velocity correlation exponent, m, is derived from an experimental curve-fit of the form $V = d^m$ and shown in Table 1 as a function of measurement location.[6] Additionally, the linear correlation coefficient and the probability of linear fit are presented. The linear correlation coefficient and the probability of linear fit relate the accuracy with which this equation models the experimental data (Taylor 1982). This experiment used from 4 to 15 points to generate a given correlation curve, with a majority of the curves based on 8 to 10 points. A probability of linear fit $\geqslant 85\%$ is required for an indication of a significant correlation.

[5] Note that discretization of this count rate algorithm into size-dependent classes constitutes the intensity deconvolution algorithm, the size measurement principle of the PCSV.

[6] The size–velocity correlations discussed in the work are all implicitly size–velocity *component* correlations. The experimental data was acquired using a single component PDPA.

Table 1 shows that a positive correlation exponent ($m > 0$) exists everywhere in the measured domain, indicating that the larger droplets move faster than small droplets throughout. Two ranges of correlation exponent exist in this table: those $\geqslant 0.5$ and those ~ 0.2. The high correlation values are restricted to the near needle regions and along principle measurement directions, i.e., in the axial direction on the spray centerline and in the radial direction near the spray periphery. Investigation of the average velocity increase over the diameter range versus the rms velocity of that data set show that values of $m < 0.2$ do not indicate a detectable correlation. Hence, a significant size–velocity correlation is assumed for positions with a correlation exponent greater than 0.2, and a high probability of linear fit.

A further examination of the raw correlation data shows a constant rms velocity exists over the measured size range for the measurement stations > 2 cm from the needle tip. This indicates that the forces governing droplet motion in this region are similar for all droplets. If this constancy were not true, the average correlation would have a greater uncertainty.

However, for the axial measurement station at ($r = 0$, $z = 5$) mm and the radial measurement station at ($r = 10$, $z = 5$) mm a size–velocity correlation plot shows a sigmoid shape. These stations exhibit a bi-modal velocity distribution. There is no correlation for very small droplets (< 2 μm) and for large droplets (> 25 μm). The rms velocity in the positive correlation region shows a nearly constant ratio of rms velocity to average velocity. The variation in rms velocity with position indicates a more complicated forcing of droplet motion near the generation point relative to that farther away. The sigmoid correlation condition is short-lived as the droplets relax to the far field trends very quickly. By the 10 mm axial station, the droplets exhibit the nearly constant rms velocity and smooth slopes as alluded to above. The time constants governing droplet production (~ 1 ms) and droplet motion (~ 10 ms) are consistent with this data (Grace and Dunn 1992b).

Additional information on the meaning of size–velocity correlations can be gathered through analytic arguments. The correlation can be described in terms of the forces acting on the droplets by using the mobility equation,

$$\mathbf{V}_{T.E.} = \mathbf{Z}\mathbf{E}$$

Here $\mathbf{Z}$ is the electrical mobility, $\mathbf{E}$ the electric field intensity and the subscripts on the terminal velocity, $\mathbf{V}_{T.E.}$. The electrical mobility can be rewritten in terms of a droplet relaxation time, τ, and the charge-to-mass ratio, q/m, as

$$\mathbf{V}_{T.E.} = \left[\frac{q}{m}\tau\right]\mathbf{E}$$

The charge-to-mass ratio and the relaxation time functionally depend on the droplet diameter. A complete correlation relationship can now be derived from the above equation by expanding $\mathbf{E}$ into its internal and external components. The external component does not depend on the droplet diameter, while the internal component depends on the diameter through the Coulombic equation. The correlation then, will have two contributing terms as seen in the following expression where the internal and external fields account for the first and second terms on the right-hand-side, respectively.

$$\mathbf{V}_{T.E.} \sim (d^{2n-1} + d^{n-1})$$

Table 1. Size–Velocity correlation power-law behavior

Measure station [r, z] mm	Axial			Radial		
	[m]	Linear correl. coeff.	Probability of lin. fit	[m]	Linear Correl. coeff.	Probability of lin. fit
(0, 05)	0.60	0.92	100	N/A	N/A	N/A
(0, 10)	0.60	0.95	85	0.60	0.36	23
(0, 30)	0.14	0.66	75	0.05	0.36	50
(0, 70)	0.11	0.90	98	0.35	0.24	37
(0, 100)	0.17	0.93	99			
(10, 05)	0.63	0.85	100	0.63	0.80	100
(10, 10)	0.53	0.89	100	0.73	0.96	100
(10, 30)	0.10	0.54	87	0.16	0.74	91
(10, 70)	0.06	0.75	96	0.19	0.87	96
(30, 05)	0.30	0.41	40	0.10	0.47	70
(30, 10)	−0.01	0.00	0	0.19	0.52	86
(30, 30)	0.27	0.88	97	0.27	0.88	97
(30, 70)	0.09	0.81	97	0.05	0.52	85
(70, 70)	0.21	0.99	100	0.19	0.94	99
(100, 70)	0.18	0.78	96	0.20	0.98	100

Here n relates the droplet charge to diameter by $(q \sim d^n)$.[7] The numerical model presented in this paper uses the maximum entropy charge model where $n=1$ (Kelly 1984). See the last paragraph in Sect. 4.1. Hence, this equation reduces to $V_{T.E.} \sim d$. Alternatively, using either the Rayleigh limit (Rayleigh 1882), the most probable or the minimum energy models (Pfeifer and Hendricks 1967), all of which have $n=1.5$, results in $V_{T.E.} \sim (d^2+d^{0.5})$. Neither charge relationship yields a correlation that matches the data well.

It should be noted that a correlation exponent around $m \sim 0.5$ can result from a dominant external field and a charge model with $n=1.5$. The measurement positions that correspond to this value of m are found in the regions where the external field is, in fact, much larger than the internal field. For conditions like $(r=1,\ z=1)$ cm where $m=0.73$, the internal field may act to increase m. The internal field does influence the radial expansion of the spray close to the needle, in regions where the axial direction sees only the dominant external field. These stations exhibit the sigmoid-type or relaxed sigmoid-type correlations that have been shown above to reduce the certainty of the correlation analysis. The decrease in m with increasing distance from the source presently cannot be accounted for.

There is some evidence of a spatial segregation of droplets, e.g., (Dunn et al. 1994 and Gañán-Calvo et al. 1994), probably due to the electric field action. The influence of segregation on the measured droplets parameters is not considered in this paper.

4 Numerical model

A numerical model was developed that predicts droplet trajectories within a monodisperse EHD fine spray by solving the steady state conservation and the steady state momentum equations along with Gauss's Law for the electrostatic potential. This was similar, in general, to other aerosol models, e.g., Filippov (1991, 1992). The model here utilizes finite differences and the equations are written using the cylindrical coordinate system with an Eulerian reference frame. The spray is axisymmetric around the needle axis; hence, the model is two dimensional (radial, r and azimuthal, z). A hyperbolic-tangent grid transformation (Fletcher 1988) was used to greatly reduce the required computation time while retaining the accuracy necessary for the high spatial gradients in the near-needle region.

The system of equations governing droplet motion in the spray: the droplet momentum, the droplet number conservation and the droplet electric potential are, respectively:

$$(\mathbf{V}\cdot\nabla)\mathbf{V} = \frac{6}{\rho\pi d^3}\left[2.78 * 10^{-9} * d * (\mathbf{E}_{ext}+\mathbf{E}_{int}) + 3\pi\mu \mathbf{V} d * (1+\tfrac{1}{6}\mathrm{Re}^{2/3})\right]$$

$$\nabla\cdot\mathbf{NV} = 0$$

$$\nabla^2\phi = -\frac{\rho_c}{\varepsilon_0} = \frac{Nq}{\varepsilon_0} = \frac{N * 2.78 * 10^{-9} * d}{\varepsilon_0}$$

Here, $\mathbf{V}$ is the droplet velocity, $\mathbf{E}_{ext}$ and $\mathbf{E}_{int}$ the external and internal electric fields, N the droplet number concentration, ϕ the droplet electric potential, ρ the liquid density of the droplet, ρ_c the space charge density (in units of charge per unit volume of spray) and d the droplet diameter. These equations are all in mksC units and the charge is evaluated using the maximum entropy charge model. This model includes the constant $(2.78 * 10^{-9})$, which results from a ratio of Lagrange multipliers used in the conservation equations for charge and energy $(-\alpha/\beta = 10^{-17}\ \mathrm{J})$ multiplied by the permittivity of free space and divided by the fundamental charge. Gravitational

[7] Note that the simple Coulombic expression for the internal electric field holds as long as the relationship between charge and diameter $(q \sim d^n)$ is the same for all diameters.

forces are several orders of magnitude below the electric and drag forces and are, therefore, neglected (Grace 1993).

4.1
Model assumptions

The assumption used in this model are: steady-state processes, a negligible air velocity, a monodisperse diameter population, a conserved droplet number and the maximum entropy charge model. These assumptions are briefly evaluated in the following paragraphs.

The steady state assumption results from experimental observations where the variation in SPC measurements from test to test is less than 5% of the average. The variation within an individual test (each ~ 150 s duration) is considered negligible by the observed constancy in the spray video image and the smooth increase in the probability density function with measurement time.

The assumption of negligible air-phase velocity decouples the droplet momentum equation from the air-phase momentum equation, greatly simplifying the model. This assumption considers the spray to be dilute such that the droplets act aerodynamically independent. An analysis by Soo (1989) considers this condition to be true when droplets are separated by more than the boundary layer thickness. Calculation of the interparticle spacing based on the droplet number concentration (separation $\sim n^{-1/3}$) shows that the droplets are, in fact, separated by several boundary layer thicknesses. Additional analysis following the method of Fuchs (1964), where the sum of the drag forces acting on the individual particles is compared to the drag force acting on the spray as a cloud, shows that the cloud drag is larger for the conditions in this spary. Therefore, again the particles are assumed to act aerodynamically independent.

The droplet conservation is predicated on the assumption that the droplets remain intact throughout the spray and are not lost through its boundary. Droplets will not coalesce due to their similar charges (Dunn and Snarski 1991), nor will they pass through the boundary in appreciable numbers due to their attraction to the electrically, grounded plate. Droplet disruption is not considered due to negligible aerodynamic forces and low evaporation rates. A monodisperse droplet population assumption makes the model computationally practical.

The charge per droplet is calculated based on the maximum entropy charge model where the charge is linearly related to the droplet diameter (Kelly 1984). The validity of this model for this particular spray has not been rigorously proven; however, it has features, e.g., a diameter-dependent approach to the Rayleigh limit, which suggest that it best models the spray charging physics relative to other common charge models, e.g., Pfeifer and Hendricks (1967). In addition, True (1980) successfully modeled an electrospray combustion plume using this charge model and experimental evidence by Dunn and Snarski (1992) suggest that this model best predicts the droplet charge in the EHD fine spray.

4.2
Solution methods and boundary conditions

The solution method for the model is straightforward. The momentum and conservation equations both use a spatial marching technique and are solved in series. The electric potential equation is then solved using the alternating direction implicit (ADI) simultaneous solution technique (Press et al. 1989). The momentum equation is solved for a velocity field, this then is input into the droplet conservation equation which is solved for the spatial number concentration. The number concentration is finally substituted into the electric potential equation to solve for the internal electric field. The total electric field is then calculated and resubstituted into the momentum equation. This procedure is then repeated until appropriate convergence is achieved. Generally, the solution to the electric potential equation required 2500 iterations on a 100×100 grid, while the resubstitution procedure required 30 iteration for convergence to less than 0.05%. Results calculated using a 50×50 grid matched those of the 100×100 grid, though the latter allows for better far-field spatial resolution.

The velocity boundary conditions result from curve-fits to the experimental data acquired along the radial line 5 mm below the needle tip. The boundary location is selected because it represents the experimental measurement station that is nearest to the needle tip, but beyond the developing region for a large part of the domain.

The droplet number concentration boundary condition is a Gaussian boundary profile which decreases to less than 5% of the centerline value at the experimentally measured spray boundary. SPC flux measurements, converted to number concentration, and video data support the selected profile. The magnitude of the centerline concentration and the model diameter result from the experimental data. They were taken to be 10^3 #/cc for a $D_{10} = 10$ μm.

The electric potential equation is elliptic; hence, the boundary conditions are specified on the entire surface surrounding the computational space. Due to the axisymmetric character of the spray, the computational space is a square with a boundary along the spray centerline. The (North) boundary, adjacent to the needle and parallel to the plate, uses a normal derivative determined in a separate program that simulates the spray as a static distribution of droplets based on experimental observations (Grace 1993). The (South) boundary along the plate is set to zero, the (West) boundary coinciding with the spray centerline, i.e., along the needle axis, specifies a zero normal derivative by symmetry, and, finally, the (East) boundary is defined by the closure of the square and set to zero (at infinity).

4.3
Droplet trajectories

Droplet trajectories are calculated from the converged velocity field. Figure 9 provides an assessment of the model through a comparison between the experimental trajectories (those derived from the digitized video images) and the numerical trajectories. Note that the digitized video images do not explicitly isolate the 10 μm droplet population (see Fig. 2). The spray boundary is also presented in Fig. 9 as determined from experimental data and numerical results. The numerical spray boundary is determined by the radial position where the droplet number concentration decreases to less than 5% of the centerline value at the grid origin.

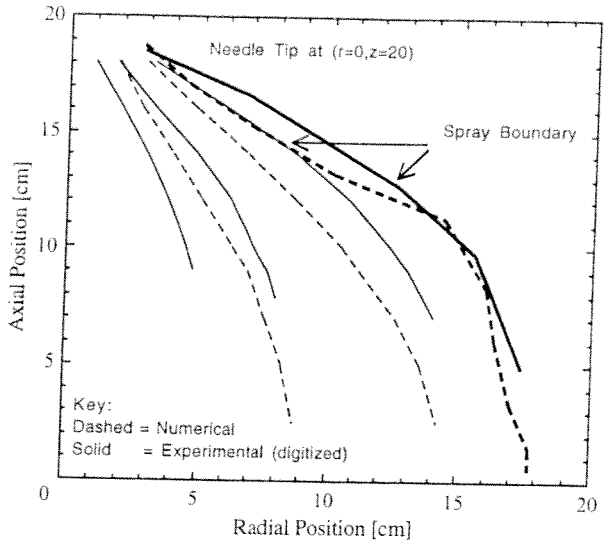

Fig. 9. Comparison between numerical and experimental droplet trajectories and spray boundary (10 μm droplets)

Figure 9 shows that the model has good qualitative agreement with the experiment. The numerical trajectories capture the expansion of the spray and the plate-ward trajectories far from the needle in the axial direction. The numerical trajectories less than $z \sim 13$ cm show excellent agreement with the video image trajectories. The numerical trajectories in the near needle region ($z > 16$) cm under predict the spray curvature, but capture the curvature far from the needle. This figure shows that the numerical spray boundary closely follows the experimental spray boundary. Note that experimental trajectories calculated without an internal electric field (using only the external electric field) do not exhibit any noticeable radial expansion; indicating the role of the internal radial electric field in the spray (Grace 1993).

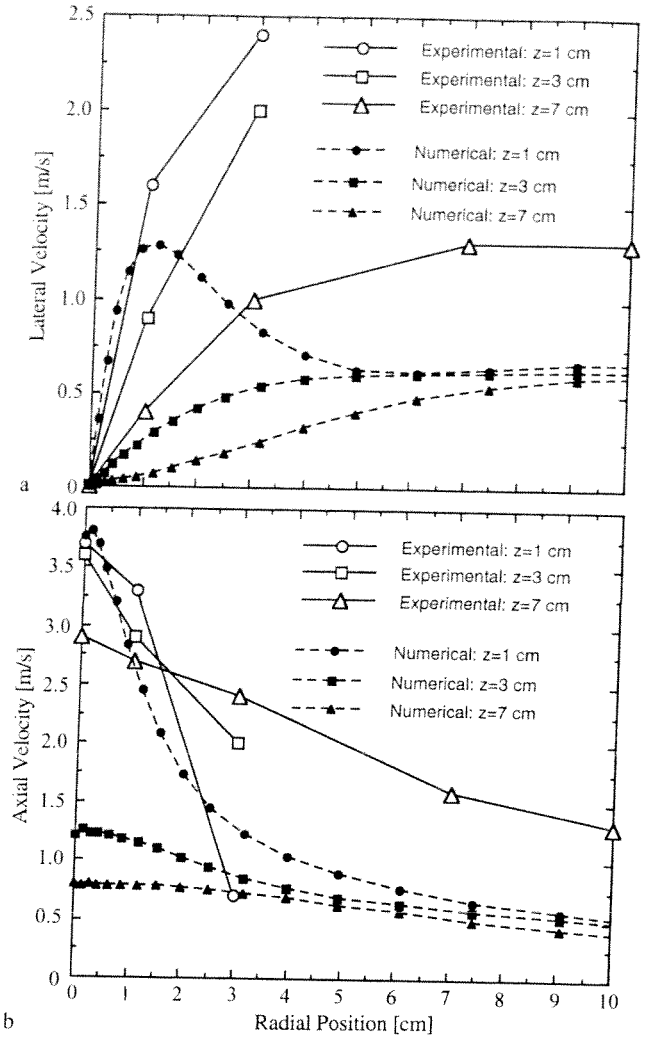

Fig. 10. **a** Comparison of experimental and numerical radial velocity versus radial position; **b** comparison of experimental and numerical axial velocity versus radial position

4.4 Droplet velocity

The numerical velocity results are compared to the experimental data in Figs. 10a, b. Both figures present only the near-field results of the numerical model. The far-field trends, e.g., the increase in the axial velocity component and the continuous increase in the radial velocity component, do not fit the scale of the experimental data.

The salient characteristics of the radial velocity component (Fig. 10a) are a maximum velocity located off-axis in the near field that moves radially from the centerline with increasing axial distance and a nearly constant, high velocity in the far field. The axial velocity component (Fig. 10b) exhibits a rapid decrease in both increasing radial and axial directions near the needle followed by a more gradual decrease in both directions with increasing distance from the needle.

The numerical velocities qualitatively capture the characteristic droplet motion in the spray. Quantitatively, the magnitudes differ appreciably from the experimental data. This difference is probably the result of a negligible air-phase velocity assumption. Though this assumption had merit, and has been used in other modelling (e.g., True 1980 and Gañán-Calvo et al. 1994) it probably does not reflect the actual spray. In fact, Gañán-Calvo, et al. (1994) report a numerical under prediction of the experimental data and propose that the discrepancy is due to entrainment. Tang and Gomez (1994) experimentally measure the entrained air velocity along their spray centerline using seed particles. These results indicate an air velocity from 10% to 30% of the local droplet velocity. Work on adapting the model to consider this two-phase flow situation is in progress.

5 Conclusions

The droplet behavior within an EHD fine spray has been characterized for the first time through a combined experimental and numerical study of the spray. Laser light-sheet visualizations of the droplets within the spray have shown that the spray expands uniformly and rapidly, with little crossing of droplet streaklines. *In situ* laser diagnostic measurements have provided more detailed information on droplet diameters, number concentrations, speeds, axial and radial velocity components and their correlations with diameter throughout the spray.

Droplet speeds were found to decrease rapidly with increasing axial distance from the capillary and then to increase beyond the spray's axial mid-plane. Droplet axial velocity components behaved similarly. The radial velocity components had maximum values off of the spray's centerline in the near-capillary region, and farther away from the capillary, they increased monotonically with increasing radial position.

All of these measured droplet speed and velocity component trends were verified by a numerical simulation of the spray. The observed increase in the droplet's speed and axial velocity component was shown to be the result of a change in sign of the axial internal electric field. The recorded droplet radial velocity component behavior in the near-capillary region was found to be governed primarily by the external electric field and by the internal electric field farther away from the capillary.

These findings for the EHD fine spray mode collectively underscore the dominant role of the external electric field in the near-capillary region and of the internal electric field farther away.

References

Aerometrics Inc. (1987) Phase Doppler particle analyzer operations manual. Mountain View, CA

Bailey AG (1988) Electrostatic spraying of liquids. New York: Wiley

Bachalo WD; Houser MJ (1984) Phase/Doppler spray analyzer for simultaneous measurements of droplet size and velocity distributions. Optical Eng 23: 583–590

Balachandran W (1991) The present and future trends in electrostatic atomization of liquids. In: Atomization and sprays 2000 Workshop, eds N. Chigier, Gaithersburg ,MD, pp. 123–139

Cloupeau M; Prunet-Foch B (1989) Electrostatic spraying of liquids in the cone-jet mode. J Electrostatics 22: 135–159

Cloupeau M; Prunet-Foch B (1990) Electrostatic spraying of liquids: main functioning modes. J Electrostatics 25: 165–184

Drozin VG (1955) The electrical dispersion of liquids as aerosols. J Col Sci 10: 158–164

Dunn PF; Snarski SR (1991) Velocity component and diameter characteristics of droplets within two interacting electrohydrodynamic sprays. Phys Fluids A 3: 492–494

Dunn PF; Snarski SR (1992) Droplet diameter, flux and total current measurements in an electrohydrodynamic spray. J Appl Phys 71: 80–84

Dunn PF; Grace JM; Snarski S R (1994) The mixing of electrically-charged droplets between and within electrohydrodynamic fine sprays. J Aerosol Sci 25: 1213–1227

Fernández de la Mora J; Loscertales IG (1994) The current emitted by highly conducting taylor cones. J Fluid Mech 260: 155–184

Filippov AV (1991) Electrostatic deposition of inertially moving charged aerosol particles onto the earthed disk. J Electrostatics 26: 81–98

Filippov AV (1992) Electrostatic deposition of a moving charged aerosol cloud onto a conducting sphere. J Aerosol Sci 23: 203–215

Fletcher CAJ (1988) Computational techniques for fluid dynamics, Vol. 2. Berlin: Springer

Fuchs NA (1964) The mechanics of aerosols. New York: Dover

Gañán-Calvo AM; Lasheras JC; Dávila J; Barrero A (1994) The electrostatic spray emitted from an electrified conical meniscus. Aerosol Sci 25: 1121–1142

Gilbert W (1600) De Magnete (p.55), translated by P.F. Mottelay. New York: Dover (1958), 89

Giles CR; Clements RM; Smy PR (1979) Flush probe studies of plasma flow over a flat plate theory J Phys D.: Appl Phys 12: 1685–1697

Grace JM; Dunn PF (1992a) Laser light-sheet visualization of the spatial evolution and mixing of coherent droplet structures. Flow visualization VI, eds. Y. Tanida, H. Miyashiro, pp. 426–430, Berlin; Springer

Grace JM; Dunn PF (1992b) Speed measurements in the developing region of an electrohydrodynamic spray using laser diagnostics. Exp Fluids 12: 261–269

Grace JM (1993) Droplet motion and control in an electrohydrodynamic fine spray. Ph.D. Dissertation, University of Notre Dame, IN

Grace JM; Dunn, PF (1994) Droplet motion in an elecrohydrodynamic fine spray. Conf. Proc. Int. Conf. Liquid Atom. and Spray Sys. Rouen, FR, 1002–1009

Grace JM; Marijnissen JCM (1994) A review of liquid atomization by electrical means. J Aerosol Sci 25: 1005–1019

Harris MT; Sissons WG; Byers CH; Basaran OA (1994) Hydrous metal oxide ceramic precursor powders by electric field enhanced atomization. Conf Proc. Fourth Intrnl. Aerosol Conf., Los Angeles, CA, 49–50

Hayati I; Bailey AI; Tadros Th F (1987) Investigations into the mechanisms of electrohydrodynamic spraying of liquids, Parts I and II. J. Colloid Interface Sci 117: 205–230

Hendricks CD (1962) Charged droplet experiments. J Colloid Interface Sci 17: 249–259

Holve DJ; Annen KD (1984) Optical particle counting, sizing and velocimetry using intensity deconvolution. Opt Eng 23: 591–603

Insitec (1989) Manual for particle counter-sizer-velocimeter * PCSV. San Ramon, CA

Jones AR; Thong KC (1971) The production of charged monodisperse fuel droplets by electrical dispersion. J Phys D: Appl. Phys 4: 1159–1166

Kelly AJ (1984) Low charge density electrostatic atomization. IEEE-IA, IA-20: 267–273

Kozhenkov VN; Fuks NA (1976) Electrohydrodynamic atomisation of liquids. Russian Chem Rev 45: 1179–1184

Lefebvre AH (1989) Atomization and sprays. New York: Hemisphere

Lord Rayleigh FRS (1882) On the equilibrium of liquid conducting masses charged with electricity. London Philos Mag and J of Sci 14: 184–186

Lüttgens U; Dülcks Th; Röllgen FW (1992) Field induced disintegration of glycerol solutions under vacuum and atmospheric pressure conditions studied by optical microscopy and mass spectrometry. Surface Sci 266: 197–203

Meesters GMH; Vercoulen PHW; Marijnissen JCM; Scarlett B (1992) Generation of micron-sized droplets from the Taylor cone. J Aerosol Sci 23: 37–49

Nadarajah S; Swift DL (1993) Generation of polydisperse aerosols of 0.5–10 μm diameter by electrospray. Conf. Proc. Amer. Assoc. Aerosol Rsrch., Oak Brook, IL, 269

O'Hern TJ; Rader DJ (1993) Practical application of In situ aerosol measurement. Halon Alternatives Tech. Working Conf., New Mexico, US DOE Report no. SAND-93-0449C

Pfeifer RJ; Hendricks CD (1967) Charge-to-mass relationships for electrohydrodynamically sprayed liquid droplets. Phys Fluids 10: 2149–2154

Press WH; Flannery BP; Teukolsky SA; Vetterling WT (1989) Numerical recipes (FORTRAN Version). New York: Cambridge University Press

Rosell-Llompart J; Fernández de la Mora J (1994) Generation of monodisperse droplets 0.3 to 4 μm in diameter from electrified cone-jets of highly conducting and viscous liquids. J Aerosol Sci 25: 1093–1119

Shackleford JR (1985) Introduction to materials science for engineers. New York: Macmillan

Smith DPH (1986) The electrohydrodynamic atomization of liquids. IEEE-IA, IA-22: 527–535

Snarski SR (1988) The interaction of electrohydrodynamically generated liquid droplets. Masters Thesis, University of Notre Dame, IN

Snarski SR; Dunn PF (1991) Experiments characterizing the interaction between two spray of electrically charged liquid droplets. Exp Fluids 11: 268–278

Soo SL (1989) Particulates and continuum- multiphase fluid dynamics. New York: Hemisphere

Tang K; Gomez A (1994) On the structure of an electrostatic spray of monodisperse droplets. Phys Fluids 6: 2317–2332

Taylor GI (1964) Disintegration of water drops in an electric field. Proc Roy Soc London, Series A 280: 383–397

Taylor JR (1982) An introduction to uncertainty analysis. Mill Valley, CA: University Science Books, Oxford University Press

True, MA (1980) Modelling of electrostatic spray plumes. Conf. Record, IEEE-IAS: 993–997

Vonnegut B; Neubauer RL (1952) Production of monodisperse liquid particles by electrical atomization. J Colloid Sci 7: 616–622

Wang SH; Chang JS; Berezin AA (1993) Atomization characteristics of electrohydrodynamic limestone–water slurry spray. J Electrostatics 30: 235–246

Zelany J (1914) The electrical discharge from liquid points and a hydrostatic method of measuring the electrical intensity at their surfaces. J Phys Rev 3: 69–91